Proceedings of the 2nd International Conference on Nanotechnology: Fundamentals and Applications
Ottawa, Ontario, Canada, 27-29 July 2011
Paper No. 360

Acicular Nanocrystals Formed Through Coprecipitation of Iron Salts in the Presence of Bovine Serum Albumin

Martin J. Hadley, Neil A. Rowson, Liam M. Grover
University of Birmingham, School of Chemical Engineering
Edgbaston, Birmingham, United Kingdom, B15 2TT
MJH048@bham.ac.uk; n.a.rowson@bham.ac.uk; l.m.grover@bham.ac.uk

ABSTRACT

In this paper we demonstrate a modification of the widely used coprecipitation of ferrous and ferric iron salts to form magnetic nanoparticles that under ambient conditions induces the formation of acicular nanoparticles with an average aspect ratio of 4:1 and a maximum extension of 700nm. Bovine Serum Albumin (BSA) was mixed with a solution of $FeSO_4$ and $FeCl_3$ (molar ratio 3:2) before NaOH was added dropwise to induce precipitation of iron oxide. Optimising conditions to prevent immediate protein globularisation and persistent network formation indicated BSA massively decelerated precipitation and crystal growth. Time-lapsed electron microscopy indicates the growth of acicular nanocrystals after 48h, highly electron-dense needles were observed after 7 days ageing *in situ* and aggregation of such structures continued over several weeks. Samples with BSA 495μMol/ml demonstrated high coercivity values which improved over time (from 0.10T after 7 days to 0.38T after 6 weeks) but could not be conclusively attributed to the acicular nanoparticles.

KEYWORDS: MNP, magnetite, acicular, protein adsorption, biomineralisation, coprecipitation acicular nanoparticle, iron oxide

1 INTRODUCTION

Biomineralisation and the coprecipitation of iron salts demonstrate surprisingly high regulation of iron oxide formation dependent on environmental conditions. In nature highly controlled magnetic nanoparticles (MNPs) are observed within bacteria (Staniland, Ward, Harrison, van der Laan & Telling, 2007), birds (Falkenberg et al., 2010) and other species and are believed to be involved in magnetoreception. Despite the plethora of examples of coprecipitation producing regulated MNPs, preferentially comprised of magnetite (Fe_3O_4), the ability to selectively change crystal growth to achieve industrially useful secondary structure has proved difficult. Acicular MNPs are particularly difficult to obtain by coprecipitation as overgrowth of Fe_3O_4 away from their preferred spherical shape is thermodynamically unfavoured (S. Chen et al., 2005).

While not well understood, biomineralisation is largely dependent on encouraging preferential crystal growth away from geologically-derived forms and this requires careful manipulation of the free-energy and enthalpy landscape to select otherwise unstable polymorphs (Raz et al., 2000). In a landmark paper in 1996 Belcher et al. (Belcher et al., 1996) demonstrated that complex pre-organised organic arrays were not necessarily required for polymorph selection, soluble proteins extracted from aragonitic and calcitic portions of mollusc shell were sufficient to preferentially select that crystal growth pathway. Recently attempts to replicate the complex MNPs observed in magnetotactic bacteria by soluble magnetosome-derived protein alone have been made with relative success (Arakaki et al., 2003).

The availability of readily formed and highly controlled MNPs is of both biomedical and fundamental interest. For many years iron oxide particles have been used as magnetic resonance imaging (MRI) contrast agents and their potential as drug delivery molecules and a part of hyperthermic cancer treatments has received much attention over the last decade (Berry and Curtis, 2003). Furthering our understanding of protein metal ion interactions should not be understated either, free-radical production has been attributed to metal adsorption by protein (Hider 2002) and an over abundance of free radicals may be linked to age-related diseases involving protein misbehaviour (Hashimoto et al., 2003).

More recently, protein separation by adsorption and later desorption on to MNPs has been demonstrated with particular emphasis on the model protein bovine serum albumin (BSA) (Peng et al, 2004). BSA has a high iron binding potential and is capable of adsorbing 8.5 moles of iron per mole of protein (Loban et al., 1997), although contrary statements are found in the literature (Collard, 2009) it is accepted that BSA possesses a ligand with particular preference for ferric iron (Fe^{3+}) (Hider, 2002). We demonstrate in this report a coprecipitation of iron salts in the presence of BSA over various concentrations from 0-1mMol/ml, an initial interaction between the protein and $Fe^{3+}Cl_3$ is observed and deposition of precipitated material is dramatically decelerated by the presence of the protein. In the absence of protein precipitated iron oxide appears plate-like under transmission electron microscopy (TEM), however acicular and haloed spheroid nanoparticles are observed for BSA 300-800μMol/ml and these samples demonstrate surprisingly high coercivity and remanance.

2 MATERIALS AND METHODS

2.1 Materials

Iron(II) sulphate heptahydrate (ReagentPlus, 99%), iron(III) chloride hexahydrate (ACS reagent, 97%) and BSA (lyophilized powder, 96%) were obtained from Sigma-Aldrich (USA). All chemicals were used as received without further treatment. Double distilled water was used throughout for dissolution.

2.2 Methods

2.2.1 Coprecipitation of Iron Oxide

Stock reagents were prepared as follows: $FeSO_4$ 2mMol/ml, $FeCl_3$ 1.3mMol, and NaOH 266mMol/ml. The Fe^{3+}:Fe^{2+} ratio is thus 2:3 and the albumin concentration approximately 1/3 of that found in bovine plasma (Fernandez et al., 1999). Except in the case of BSA magnetic stirring at 750rpm for 5 min was sufficient for full dissolution – 30 min stirring under gentle heating was required for the BSA stock. BSA, $FeSO_4$ and then $FeCl_3$ were added to a reaction vessel before dropwise addition of NaOH over 1 min to induce precipitation. The resulting solution was then sealed and allowed to age under ambient conditions. Protein concentration was varied from 0-1mMol/ml. All reagents were used within three days of preparation, continuous magnetic stirring at 200rpm of the BSA stock solution prevented sedimentation.

2.2.2 BSA Adsorption Properties

The adsorption of iron ions by the BSA molecule, and BSA adsorption by pre-formed magnetite was measured by a QuantiPro BCA Assay Kit (Sigma Aldrich), assuming Cu^{2+} reduction by the protein in alkaline medium was effectively impaired due to iron binding (Smith et al., 1985). The concentration of free BSA observed at various stages in sample preparation was compared with the stock solution used for assays, 27μMol/ml. Time-lapse measurements of iron in the sample supernatant were achieved by atomic absorbance spectroscopy (AAS).

2.2.3 Characterisation of Deposited Material

Initial characterisation of precipitated crystal morphology was carried out using TEM by a Jeol 1200EX instrument operated at 80keV, additional imagery and energy dispersive x-ray spectroscopy was achieved by Phillips TECNAI F20 operated at 200keV. For all images 20µl of solution was deposited by pipette on to a carbon film copper grid (Agar). Iron oxide identification was investigated by x-ray powder diffraction (XRD) using a Bruker D8 ADVANCE diffractometer, and magnetic properties were measured at room temperature by vibrating sample magnetometry (VSM) (Lakeshore, 7400).

3 RESULTS AND DISCUSSION

3.1 Coprecipitation of Iron Oxide

Initial investigations of the affect of BSA inclusion in iron salt coprecipitation demonstrated a visually evident interaction between $FeCl_3$ and the protein solution during sample preparation. Upon addition of $FeCl_3$ the solution became cloudy and rust coloured, and gelatinous white globular material precipitated immediately but dissolved within 5 min of formation. This interaction is attributed to Fe^{3+} binding by BSA (Hider, 2002). The presence of $FeSO_4$ produced no visibly evident difference but BCA assay indicated an inhibited interaction (Figure 1).

Sodium hydroxide was then added to the BSA and iron salt solution immediately (before dissolution of the precipitated gelatinous material could occur) and colour change was immediate from the first drop and the globular material disappeared within 10 s. For BSA 300-800µMol/ml, after ¾ of the NaOH solution was added denser white globular material precipitated near the solution surface to where it proceeded to rise and dissipated within 5 min. The final colour of the solution was similar to that of urea. The samples remained stable over approximately 48h, after which time black iron oxide began to deposit from a dark brown supernatant and over 48 h to 4 days this supernatant became clearer but with a slight blue hue. In the absence of protein the addition of NaOH to iron salts induced immediate precipitation and deposition of dark black material, the supernatant appeared clear and the samples were stable over 6 weeks.

This report focuses primarily on the acicular nanoparticles observed to form under coprecipitation of iron salts and BSA 495µMol/ml. The experiment is relatively sensitive to protein concentration, <300µMol/ml results in much faster deposition of material from solution (<24 h), and these samples do not demonstrate haloed spheroids or acicular nanoparticles suggesting that decelerated crystal growth is responsible for the morphological change observed (Combes and Rey, 2002; Davey, 1976). For BSA <900µMol/ml the precipitation of globular material during addition of NaOH is no longer observed. Instead the solution enters a three phase equilibrium; relatively clear fluid appears below a band of dark brown material which itself appears below a light yellow fluid. After 7 days material is not deposited, the solution displays a gentle gradient from dense dark brown to almost clear at the top, after 6 weeks the solution appears jet black with no deposited material evident by visual inspection or TEM.

The reported acicular nanoparticle formations in this study were not observed when the Fe^{3+}:Fe^{2+} ratio was inverted to 3:2, this is surprising as a higher Fe^{3+} concentration is typically considered to compensate for the rapid oxidation of Fe^{2+} during precipitation allowing for increased precipitation of $Fe_2^{3+}O_3$, required for spinel ferrite structures such as magnetite (Chen et al., 2005; Tebble and Craik, 1969). Furthermore, the application of gentle nitrogen bubbling during precipitation to displace oxygen is common in the literature, however there was no noticeable change in crystal morphology after 6 weeks to warrant nitrogen use.

3.2 BSA Adsorption Properties

The apparent precipitation of gelatinous material upon addition of $FeCl_3$ to $FeSO_4$ and BSA during coprecipitation was attributed to iron adsorption by the protein, this is evidenced by the reported high iron binding potential of BSA (Hider 2002b; Collard 2009) and BCA assay data (Figure 1). Using a standard

curve of 0-30μMol/ml the absorbance at 562nm of a 27μMol/ml BSA solution was measured and compared with various samples. In the case of iron salts it is assumed the reduced 562nm absorbance is due to iron binding preventing Cu^{2+} reduction rather than precipitation due to acidity resulting in conformational change preventing the biuret reaction.

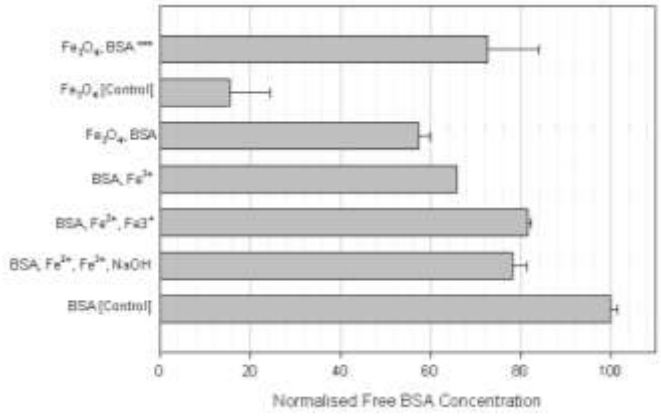

Figure 1: Approximate relative BSA adsorption or absorption of various stages in iron oxide precipitation. Preformed magnetite was assayed separately so as to account for the iron oxides' assumed 562nm absorbance, approx. 18% of BSA [Control] (27μMol/ml). All errors are calculated by standard deviation of five sample repeats. *** The 562nm absorbance of Fe_3O_4 [Control] has been added to Fe_3O_4, BSA.

Supernatant levels of iron were analysed by AAS after 7 and 16 days against a standard curve from 5-100ppm, yielding 8ppm and <5ppm respectively. In total each sample contained approximately 0.1725mg/ml (75ppm), indicating that within 7 days almost 90% of iron was incorporated into the deposited material and >95% after 16 days.

3.3 Characterisation of Deposited Material

The deposited material in all samples from BSA 0-800μMol/ml demonstrated attraction to an applied magnetic field, such that if strongly agitated to re-disperse the material a barium ferrite magnet was capable of collecting all material to the side of the sample container. Further agitation fully re-dispersed the material after the field had been removed. Quantitative measurements by VSM (see Figure 2) demonstrate that as the material is allowed to age *in situ* from day 7 to day 16 both the sample coercivity and remanance increase markedly from 0.10Oe to 0.38T and 0.012T to 0.044T, respectively. This suggests a crystal ripening process: an increased coercive field is indicative of either an increase in crystal size or shape anisotropy from overgrowth along a particular axis (Gregg et al., 2006; Staniland et al., 2008). While AAS does indicate continued removal of iron from the supernatant from day 7 to 16, itself evidence of a mass limited transport growth mechanism, the change is less than 8ppm compared to a total reservoir of 75ppm and therefore unlikely to be the main mechanism behind the dramatic change in hysteresis behaviour. The shape profile of the hysteresis loops in Figure 2 appears to be tending toward a square loop, indicating superparamagnetic particles are no longer the main contributing factor to the sample magnetisation and that shape anisotropy is prominent. Further time-lapse VSM data may confirm this.

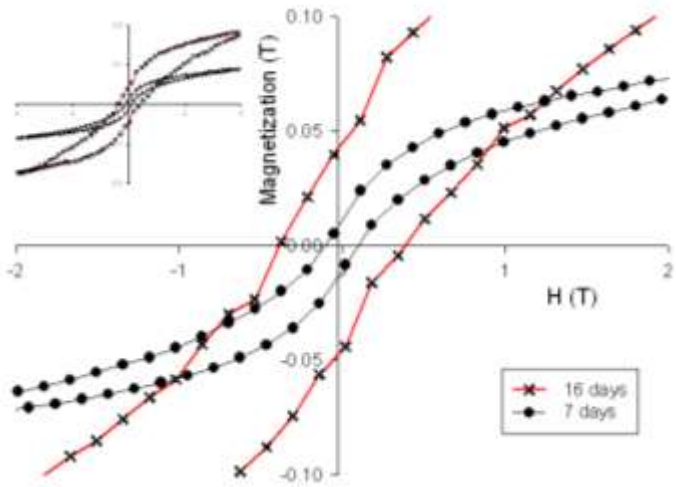

Figure 2: Hysteresis loops showing characteristic changes in the magnetic properties of the precipitated material over time. There is a notable change in hysteresis behaviour that may be attributed to shape anisotropy in maturing acicular particles. Inset: complete hysteresis loops.

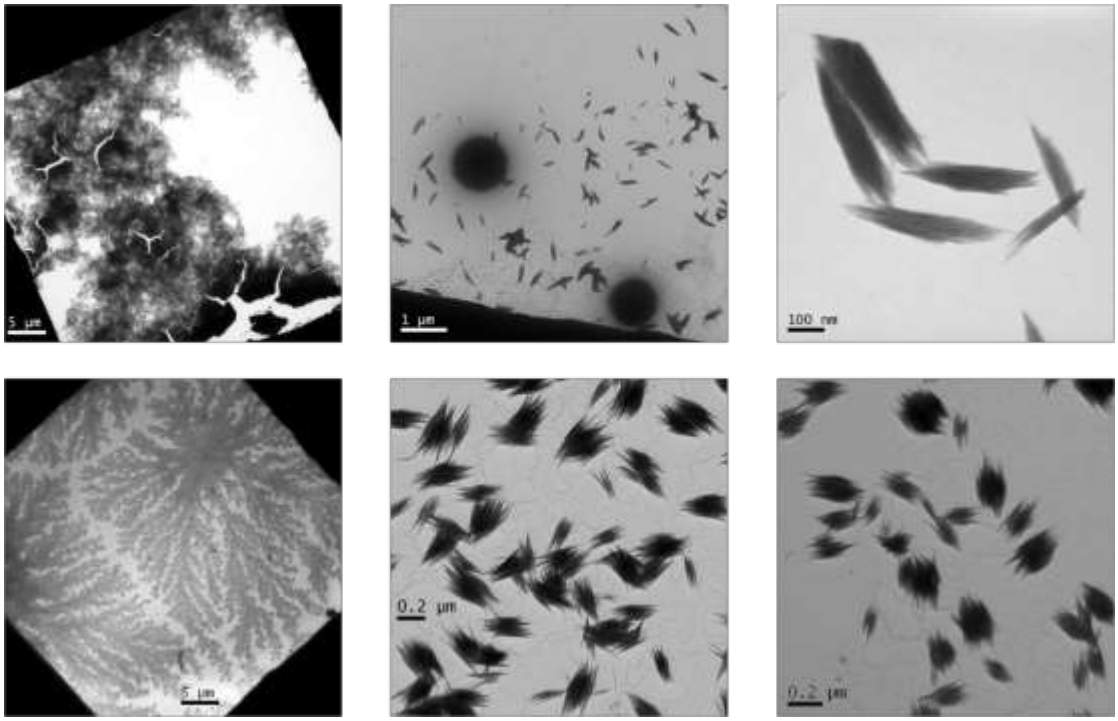

Figure 3: TEM images showing time evolution and variety of precipitated material. Top images, left to right: Control sample after 24 h, BSA 495µMol/ml after 7 days, and BSA 495µMol/ml after 7 days. Bottom images, left to right: BSA 270µMol/ml after 24 h demonstrates typical fractal structure (dissipates within 3 days), BSA 495µMol/ml after 6 weeks, and BSA 495µMol/ml after 6 weeks.

In the absence of protein the coprecipitation routine results in the immediate deposition of dark black material that also responds to applied magnetic fields, TEM imagery identifies two main species: poorly formed particles (<10nm) and structure-less plate-like material – Figure 3 shows the appearance of such a control after 24 h ageing, at 6 weeks the appearance of the sample is much the same. In the presence of protein the sample observes a more complicated growth process. For BSA 200-800µMol/ml a fractal and non-crystalline structure is identified in all samples with some apparent darker particles

within, suggesting a protein-matrix within which crystalline material is precipitated (see Figure 3). These unusual structures are evident for almost 48 h, after which time poorly formed and densely aggregated particles are observed for BSA <300μMol/ml. Two unusual particle species are observed for BSA 300-800μMol/ml but are particular evident at 495μMol/ml, as shown in Figure 3; acicular electron dense particles ranging from 400-700nm with aspect ratios of 4:1 and haloed spheroids approximately 1μm in diameter. The acicular particles display evidence of polycrystallinity, particularly evident in the higher magnification images in Figure 3 and this preferential crystal growth may offer an explanation for increasing sample coercivity over time. There is no observed growth in haloed spheroid population over 6 weeks.

Whole sample crystallographic data was inaccessible by XRD, vacuum dried sample displayed plastic film-like properties rather than dry powder which is attributed to high protein concentration which combined with small crystal size masks identifiable Bragg reflections difficult to resolve. EDX showed characteristic compositional differences between the two particle species, attributing sulphur to cysteine methionine in BSA there is a much higher protein concentration in the spheroids than in the acicular particles (see Figure 4). Surprisingly little iron is observed by EDX in the majority of particles analysed, it is therefore difficult to attribute the widening of hysteresis loops to a particular species.

The included TEM images (Figure 3) characterise the majority of observed material in all samples, should an unobserved species be iron heavy and thus responsible for high coercivity it is clear that the presence of BSA is responsible due to distinct morphological differences between these samples and the control. Furthermore, both acicular and spheroid particle populations are large enough that if they were not ferrimagnetic their deposition would be evident after agitation and application of magnetic field but this was not observed.

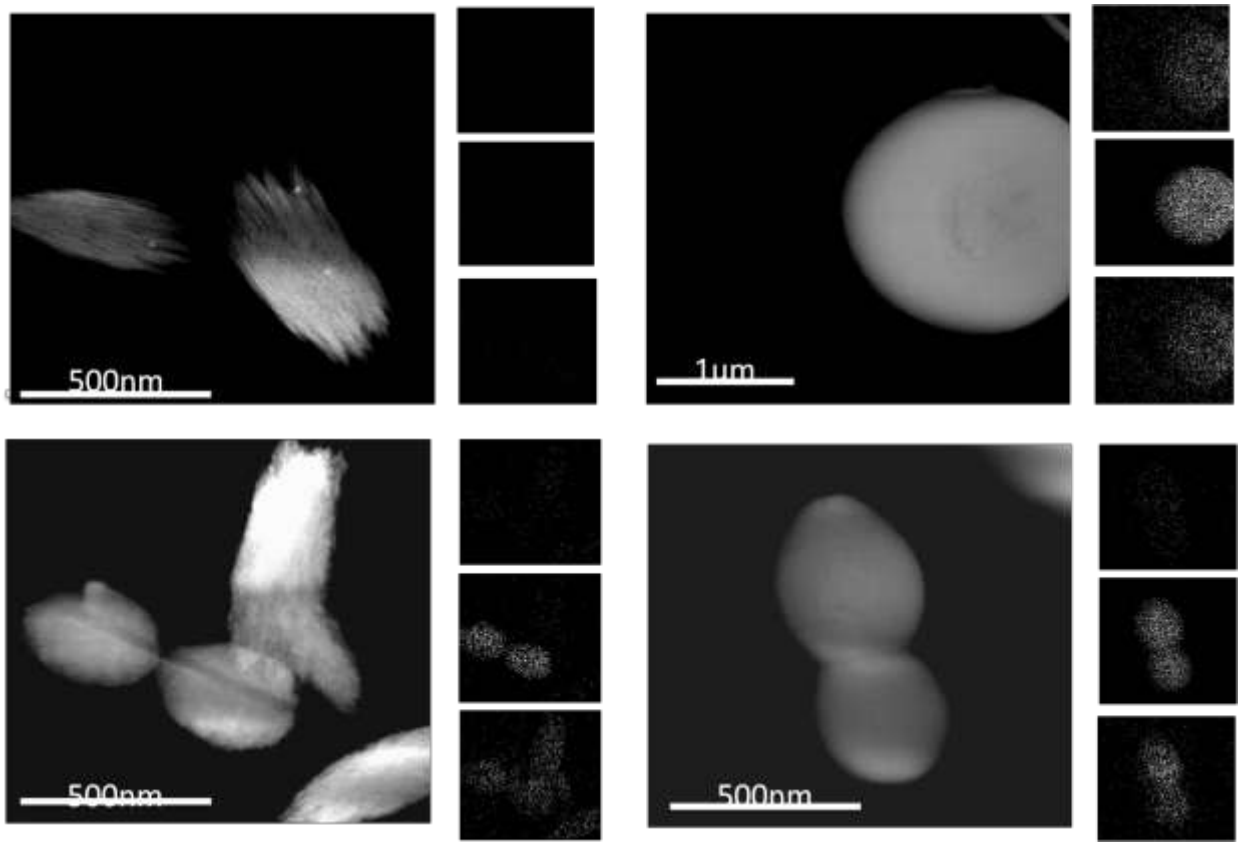

Figure 4: STEM images with EDX element maps. Top Row: Nanoparticles imaged after 7 days of ageing. Bottom Row: Nanoparticles imaged after 14 days. For all images EDX element maps from top to bottom; iron, sulphur, oxygen.

4 CONCLUSIONS

The coprecipitation of iron salts in the presence of low BSA concentration induces the growth of two distinct particle species, haloed spheroids and polycrystalline acicular particles. While the former remains essentially stable, the latter matures by preferential aggregation (Figure 3) and increasing iron, oxygen and sodium concentration. Magnetic characterisation indicates that sample maturity corresponds to increased coercivity and remanance however there is insufficient evidence to link this directly to acicular particle maturity. This study further demonstrates preferential binding of Fe^{3+} to BSA and that soluble protein in decelerated crystal growth and morphological changes. The magnetism of the sample is attributed to iron oxide, which must be of the form $Fe_2^{3+}O_2$ but identification of this material is difficult, there is perhaps insufficient iron detected by EDX in the acicular particles to consider them as iron oxide crystal in their entirety – nanoparticle particle may be incorporated into these structures, however such particles would likely display low coercivity. The availability of readily formed acicular MNPs with high coercivity has potential applications in biomedicine and high density magnetic storage devices.

5 ACKNOWLEDGEMENTS

The author would like to acknowledge the Biotechnology and Biological Sciences Research Council (BBSRC) for funding this project.

REFERENCES

Arakaki A. and Webb J. and Matsunaga T. (2003). A Novel Protein Tightly Bound to Bacterial Magnetic Particles in Magnetospirillum Magneticum Strain AMB-1. The Journal of Biological Chemistry, 278(10), 8745-50.

Belcher A.M. and Wu X.H. and Christensen R.J. and Hansma P.K. et al. (1996) Control of Crystal Phase Switching and Orientation by Soluble Mollusc-Shall Proteins. Nature, 381(1), 56-58.

Berry C.C and Curtis A.S.G. (2003). Functionalisation of magnetic nanoparticles for applications in biomedicine. Journal of Physics D: Applied Physics, 36(13), R198-R206.

Chen S. and Feng J. and Guo X. and Hong, J. and Ding, W. (2005). One-step Wet Chemistry for Preparation of Magnetite Nanorods, Materials Letters, 59, pp. 985 - 988.

Collard K.J. (2009). Iron Homeostasis in the neonate. Pediatrics, 123(4), 1208-16.N

Combes C. and Rey C. (2002). Adsorption of Proteins and Calcium Phosphate Materials Bioactivity. Biomaterials, 23(13), 2817-23.

Davey R. (1976). The Effect of Impurity Adsorption on the Kinetics of Crystal Growth from Solution. Journal of Crystal Growth, 34(1), 109-119.

Falkenberg G. and Fleissner G. and Schuchardt K. and Kuehbacher M. et al. (2010). Avian Magnetoreception: Elaborate Iron Mineral Containing Dendrites in the Upper Beak seem to be a Common Feature of Birds. PloS one, 5(2), e9231.

Fernandez S and Rodriguez J. and Padilla A. (1999). Removal Concentration and Desalination of Bovine Seroalbumin (BSA) with Membrane Technology. Desalination, 126(1-3), 95-100.

Gregg K.A. and Perera, S.C. and Lawes G. and Shinozaki S. and Brock S. L. (2006). Controlled Synthesis of MnP Nanorods: Effect of Shape Anisotropy on Magnetization. Chemistry of Materials, 18(4), 879-886.

Hashimoto M. and Rockenstein E. and Crews L. and Masliah E. (2003). Role of Protein aggregation in Mitochondrial Dysfunction and Neurodegeneration in Alzheimer's and Parkinson's diseases. Neuromolecular medicine, 4(1-2), 21-36.

Hider R.C (2002). Nature of Nontransferrin-bound Iron. European journal of clinical investigation, 32 Suppl 1, 50-4.

Jiang W. and Sun Z. and Li F. and Chen K. et al. (2010). A Novel Approach to Preparing Magnetic Protein Microspheres with Core-shell Structure. Journal of Magnetism and Magnetic Materials, 323(5), 435-439.
Loban A. and Kime R. and Powers H. (1997). Iron-binding Antioxidant Potential of Plamsa Albumin. Clinical Science, 95, 445-451.
Peng Z.G. and Hidajat K. and Uddin M. S. (2004). Adsorption of Bovine Serum Albumin on Nanosized Magnetic Particles. Journal of Colloid and Interface Science, 271(2), 277-83.
Raz S. and Weiner S. and Addadi L. (2000). Formation of High-Magnesian Calcites via an Amorphous Precursor Phase: Possible Biological Implications. Advanced Materials, 12(1), 38-42
Smith P.K and Krohn R.I and Hermanson G.T. and Mallia A.K. et al. (1985). Measurement of Protein Using Bicinchoninic Acid. Analytical Biochemistry, 150(1), 76-85.
Staniland and S. and Ward B. and Harrison A. and van der Laan G. and Telling N. (2007). Rapid Magnetosome Formation Shown by Real-time X-ray Magnetic Circular Dichroism. Proceedings of the National Academy of Sciences of the United States of America, 104(49), 19524-8
Staniland S. and Williams W. and Telling N. and van der Laan G. et al. (2008). Controlled Cobalt Doping of Magnetosomes in vivo. Nature nanotechnology, 3(3), 158-62
Tebble, R. S and Craik, D. J. (1969) Magnetic Materials, London, Wiley-Interscience.